Available online at www.sciencedirect.com
ScienceDirect
Journal of Physics and Chemistry of Solids 68 (2007) 1836–1840
JOURNAL OF PHYSICS AND CHEMISTRY OF SOLIDS
www.elsevier.com/locate/jpcs

Synthesis and characterization of room-temperature ferromagnetism in Fe- and Ni-co-doped In_2O_3

Xing Li[a,b], Changtai Xia[a,*], Guangqing Pei[a,b], Xiaoli He[c]

[a]*Shanghai Institute of Optics and Fine Mechanics, Chinese Academy of Sciences, Jia Ding, Shanghai 201800, PR China*
[b]*Graduate School of the Chinese Academy of Sciences, Beijing 100039, PR China*
[c]*Key Laboratory of Materials Physics, and Anhui Key Laboratory of Nanomaterials and Nanostructures, Institute of Solid State Physics, Chinese Academy of Sciences, Hefei 230031, PR China*

Received 5 January 2007; accepted 7 May 2007

Abstract

Observation of room-temperature ferromagnetism in Fe- and Ni-co-doped In_2O_3 samples $(In_{0.9}Fe_{0.1-x}Ni_x)_2O_3$ $(0 \leqslant x \leqslant 0.1)$ prepared by citric acid sol–gel auto-igniting method is reported. All of the samples with intermediate x values are ferromagnetic at room-temperature. The highest saturation magnetization ($0.453\,\mu_B$/Fe + Ni ions) moment is reached in the sample with $x = 0.04$. The highest solubility of Fe and Ni ions in the In_2O_3 lattice is around 10 and 4 at%, respectively. The 10 at% Fe-doped sample is found to be weakly ferromagnetic, while the 10 at% Ni-doped sample is paramagnetic. Extensive structure including Extended X-ray absorption fine structure (EXAFS), magnetic and magneto-transport including Hall effects studies on the samples indicate the observed ferromagnetism is intrinsic rather than from the secondary impurity phases.

Keywords: A. Magnetic materials; B. Sol–gel growth; C. EXAFS; D. Magnetic properties

1. Introduction

Recently, room-temperature ferromagnetic semiconductors have boosted great interest due to their potential spintronics applications. Since the discovery of ferromagnetism in Mn-doped GaAs [1], considerable research has focused on finding new semiconductors exhibiting ferromagnetic feature [2–5]. Generally, diluted magnetic semiconductors (DMSs) are formed by doping some amount of magnetic transition metal ions into the host lattice of a semiconductor. However, due to the small solubility of magnetic ions in the host lattice, ferromagnetism in some cases is attributed to magnetic impurities [6]. Therefore, a search for new candidates with intrinsic ferromagnetism for DMS oxide materials is crucial.

Since In_2O_3-based compounds have been widely used as transparent conductors, they are attractive for the semiconductor industries. Recently, Yoo et al. [7] and He et al. [8] have reported the room-temperature ferromagnetism obtained in both bulk and thin film Fe- and Cu-co-doped In_2O_3 samples. The solubility of Fe atoms in In_2O_3 lattice was found to be around 20 at%, which is very high. Peleckis et al. [9] reported the T_c for Mn-doped In_2O_3 to be only 46 K, but room-temperature ferromagnetism has been found in Fe- and Mn-co-doped In_2O_3 bulk samples [10]. They also found that Fe-doped In_2O_3 samples show a trace of paramagnetic behavior at room-temperature, which contradicts the results reported by Shim et al. [11] Moreover, Peleckis et al. [12] also obtained room-temperature ferromagnetism in Ni-doped In_2O_3 and ITO bulk samples, but the ferromagnetism is very weak. Therefore, we expected that when In_2O_3 was co-doped with Fe and Ni, enhanced ferromagnetism would be obtained. In this paper, we report on the observation of enhanced room-temperature ferromagnetism in Fe- and Ni-co-doped In_2O_3 polycrystalline samples and the origin of ferromagnetism in this system.

*Corresponding author. Tel.: +86-21 69918482; fax: +86 21 69918607.
E-mail address: Xia_CT@siom.ac.cn (C. Xia).

0022-3697/$ - see front matter © 2007 Elsevier Ltd. All rights reserved.
doi:10.1016/j.jpcs.2007.05.019

2. Experimental procedure

Polycrystalline samples of $(In_{0.9}Fe_{0.1-x}Ni_x)_2O_3$ ($0 \leqslant x \leqslant 0.1$) were fabricated by the citric acid sol–gel auto-igniting method. Starting materials of $InCl_3 \cdot 4H_2O$ (99.99%), Fe $(NO_3)_3 \cdot 9H_2O$ (A.R.), Ni $(NO_3)_2 \cdot 9H_2O$ (A.R.), $C_6H_8O_7 \cdot H_2O$ (A.R.) were weighed and dissolved in distilled water in corresponding ratio to obtain 200 ml aqueous solution. And then add some amount of dilute nitric acid to control the pH value in a range of 2–3, with the ratio of citric acid to nitrate being 1.5:1. The solution was continuously stirred at 70 °C for several hours till it turned to sol, which was then transformed into sticky gel through continuously stirring at 85 °C. Then the gel was subsequently heated to 230 °C when the auto-igniting process occurred. The obtained powders were sintered in a muffle furnace at a temperature of 500 °C for 10 h. The bulk sample with $x = 0.04$ used for Hall measurement was obtained by pressing the sintered powder into a rectangular-shaped pellet and sintered at 1000 °C for 20 h to decrease its bulk resistance. The phase and crystal structure of samples were analyzed by means of X-ray diffraction (XRD) technique using Ni-filtered CuKα radiation (Rigaku Corp.; 40 kV, 300 mA). Extended X-ray absorption fine structure (EXAFS) were performed using synchrotron radiation at the National Synchrotron Radiation Laboratory. The magnetic properties and Hall Effect measurement were performed on the physical properties measurement system (PPMS-9; Quantum Design).

3. Result and discussion

The XRD pattern for all the samples can be indexed based on the unit cell of a cubic In_2O_3 and a hexagonal In_2O_3. The measured and standard diffraction patterns are shown in Fig. 1. The standard XRD patterns for hexagonal In_2O_3, $NiFe_2O_4$, Fe_3O_4, Fe_2O_3, and as-prepared cubic In_2O_3 are also shown at the bottom of the figure. The structures of all the Fe- and Ni-co-doped samples are consistent with that of the hexagonal and cubic In_2O_3, and no other impurity phases can be found; while only Ni-doped sample has no trace of hexagonal In_2O_3 phase. The emerging of hexagonal In_2O_3 is consistent with Parent's work [13], and according to Wycoff, the phase transfer from cubic to hexagonal is favored when a foreign atom, M, with smaller ionic radius than indium is planted in the cubic In_2O_3 network, especially when $r\ (M)/r\ (O^{2-}) = 0.6$ [14]. The Fe ions fit these two conditions: the ionic radius of Fe^{3+} in six-coordinated configuration is 0.69 Å, smaller than In^{3+}, and $r\ (Fe^{3+})/r\ (O^{2-}) = 0.58$, almost equal to 0.6. Due to the fact that the hexagonal In_2O_3 phase has already emerged in the sample $(In_{0.9}Fe_{0.1})_2O_3$ while no hexagonal In_2O_3 phase can be found in only Ni-doped sample $(In_{0.9}Ni_{0.1})_2O_3$, we could propose an assumption: if all of the Fe and Ni atoms have been incorporated into In_2O_3 host lattice, parts of Fe atoms inhabit in hexagonal In_2O_3 lattice while Ni atoms prefer to keep in cubic lattice.

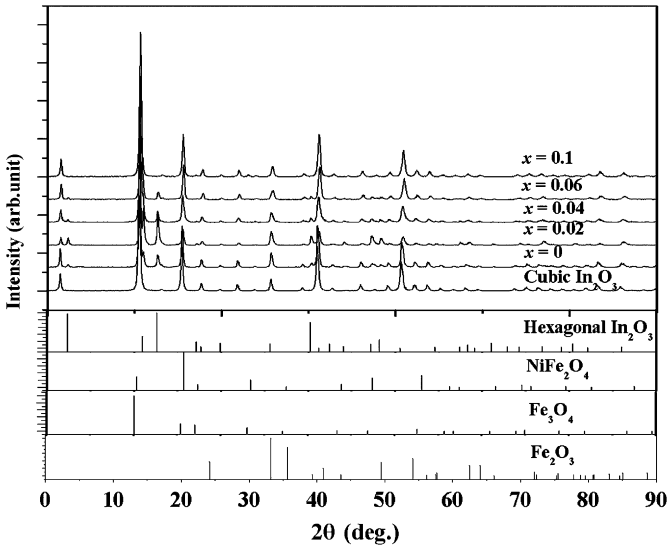

Fig. 1. XRD pattern of $(In_{0.9}Fe_{0.1-x}Ni_x)_2O_3$ and pure cubic In_2O_3 samples. The intensity bars from standard diffraction patterns for bulk hexagonal In_2O_3, $NiFe_2O_4$, Fe_3O_4, and Fe_2O_3 are also included for comparison.

And EXAFS analyses discussed later can confirm this assumption.

For the reason that XRD is a "bulk" technique and its sensitivity cannot help us to determine the existence of secondary sediment phases, we employed the EXAFS to investigate the local environment as well as the valences of Fe and Ni ions. The near-edge structure at Fe and Ni K-edges for samples with $x = 0$, 0.02, 0.04 along with the reference spectra of Fe, α-Fe_2O_3, Fe_3O_4, Ni, NiO powders clearly tell us the valences of Fe and Ni ions are +3, +2, respectively, as shown in Figs. 2(a) and 3(a). This can rule out the existence of Fe_3O_4 clusters. A typical Fourier-transformed Fe K-edge EXAFS spectrum of samples with $x = 0$, 0.02 is compared in Fig. 2(b) with Fe and α-Fe_2O_3 powders. The first important experimental result is that the radial distribution function (RDF) results of samples with $x = 0$, 0.02 are very similar to that of reference sample α-Fe_2O_3, while they are completely different from Fe powder. This can exclude the existence of Fe clusters. Furthermore, close examination between samples with $x = 0$, 0.02, and α-Fe_2O_3 reveals some characters. One is that the first major peaks in the RDFs of the samples with $x = 0$, 0.02 are clearly composed of two contributions, which indicates the existence of hexagonal In_2O_3, consistent with Ref. [13]. This can also be confirmed by XRD patterns and support our previous assumption. The other is that the first major peak position of sample with $x = 0$ and α-Fe_2O_3 is almost equal. We can conclude that parts of Fe atoms exist in Fe_2O_3. The emerging of a small shoulder (indicated by the array) in the second major peak also supports this fact, which shows that the solubility of Fe atoms in In_2O_3 host lattice is around 10 at%, which is half of that reported in Ref. [8]. However, for the sample with $x = 0.02$, the first major peak position has a little shift to

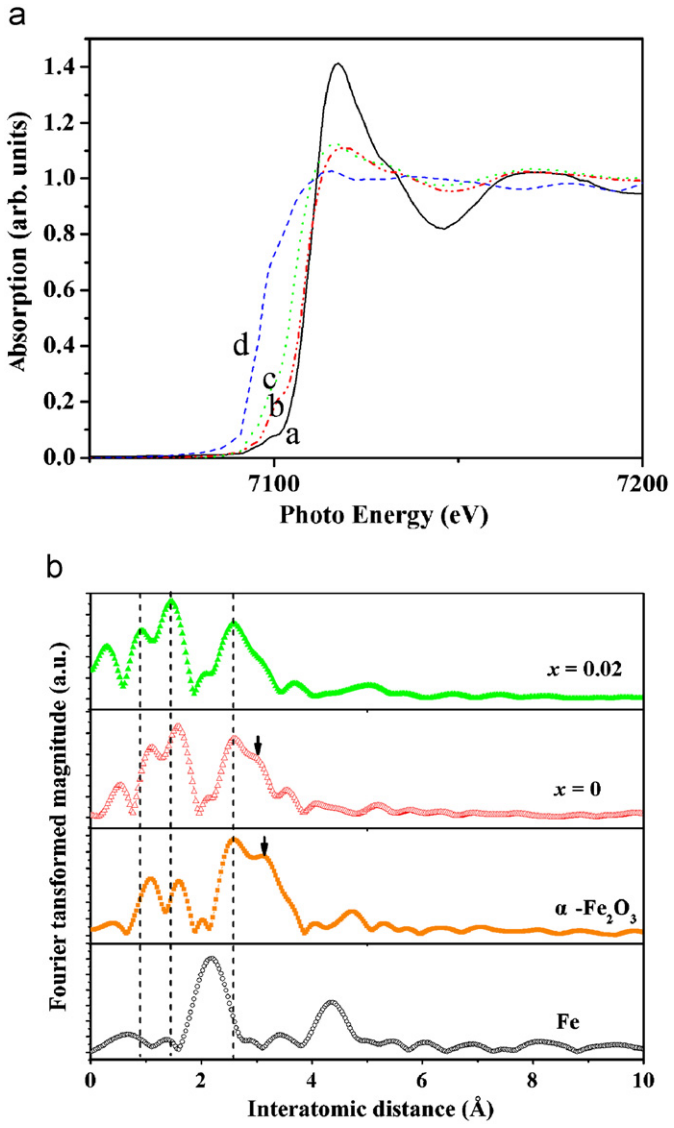

Fig. 2. (a) The near-edge structure at Fe *K*-edge for the sample $(In_{0.9}Fe_{0.08}Ni_{0.02})_2O_3$ (a) and reference samples of α-Fe_2O_3 (b) and Fe (c) and Fe_3O_4 (d); (b) comparison of Fourier transforms from Fe *K*-edges for as-prepared samples $(In_{0.9}Fe_{0.1-x}Ni_x)_2O_3$ and reference samples Fe, α-Fe_2O_3.

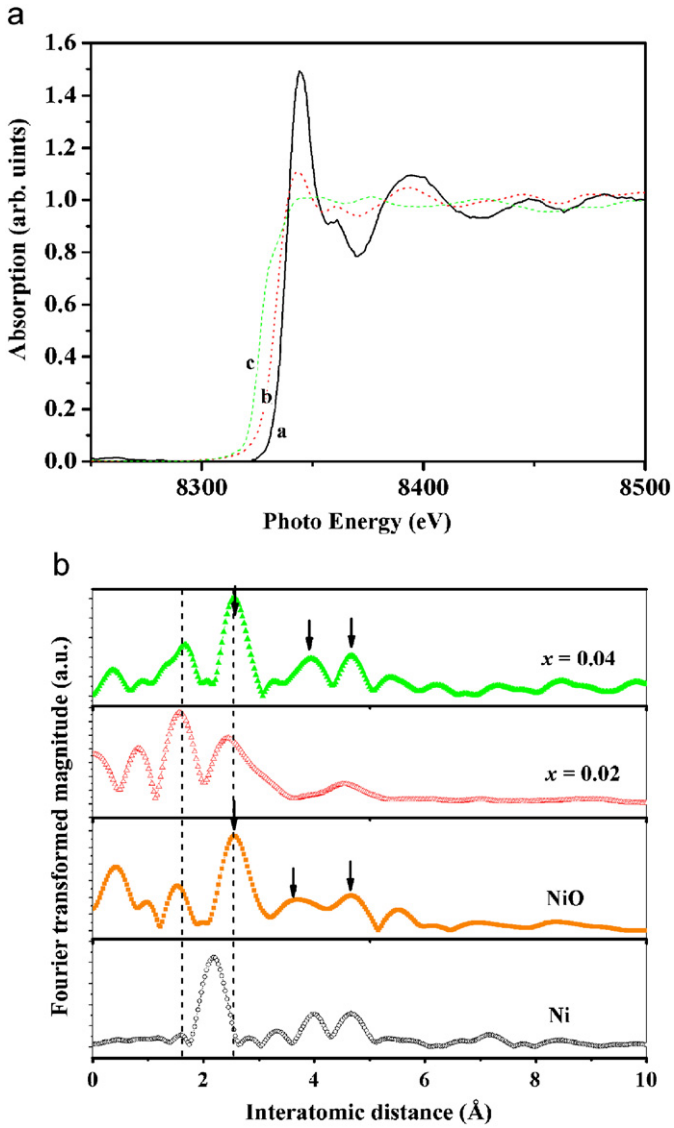

Fig. 3. (a) The near-edge structure at Ni *K*-edge for the sample $(In_{0.9}Fe_{0.08}Ni_{0.02})_2O_3$ (a) and reference samples of NiO (b) and Ni (c); (b) comparison of Fourier transforms from Ni *K*-edges for as-prepared samples $(In_{0.9}Fe_{0.1-x}Ni_x)_2O_3$ and standard samples Ni, NiO.

smaller interatomic distance compared with the sample with $x = 0$ and α-Fe_2O_3. Moreover, the small shoulder disappeared in the sample with $x = 0.02$. These suggest that in the sample with $x = 0.02$, the local structure of Fe atoms is completely different from that of α-Fe_2O_3, which indicates that Fe atoms have already incorporated into In_2O_3 host lattice successfully. The Fourier-transformed Ni *K*-edges are compared in Fig. 3(b) with reference Ni, NiO powders. The first important experimental result is that the RDF results of the two samples are completely different from Ni powder, which rules out the existence of Ni clusters. The other is that the RDF results of sample with $x = 0.04$ and NiO are very similar, both of which appear fcc structure (as described by the array), while for the sample with $x = 0.02$, the RDF results show similar bcc structure, which further confirms our previous assumption that Ni atoms exist in cubic lattice. We could draw a conclusion from this result that NiO clusters have already formed in the sample with $x = 0.04$ and maximum solubility of Ni atoms in the cubic In_2O_3 network is around 4 at% in our sample.

Fig. 4(a) shows magnetization (M) versus applied magnetic field (H) at room-temperature for samples with $x = 0.02$, 0.04 and 0.06. All samples appear ferromagnetic at room-temperature and similar results can also be found in Ref. [12]. It can be seen from Fig. 4(a) that, as the x value increases, enhanced ferromagnetism is obtained characterized by higher saturation magnetization (M_s). The M_s in our samples with $x = 0.02$, 0.04, 0.06 is 0.58 (0.28 μ_B/Fe + Ni ions), 0.95 (0.453 μ_B/Fe + Ni ions), 0.93 (0.442 μ_B/Fe + Ni ions) emu/g, respectively, much higher than that reported 0.017 emu/g in the Ni-doped In_2O_3, ITO

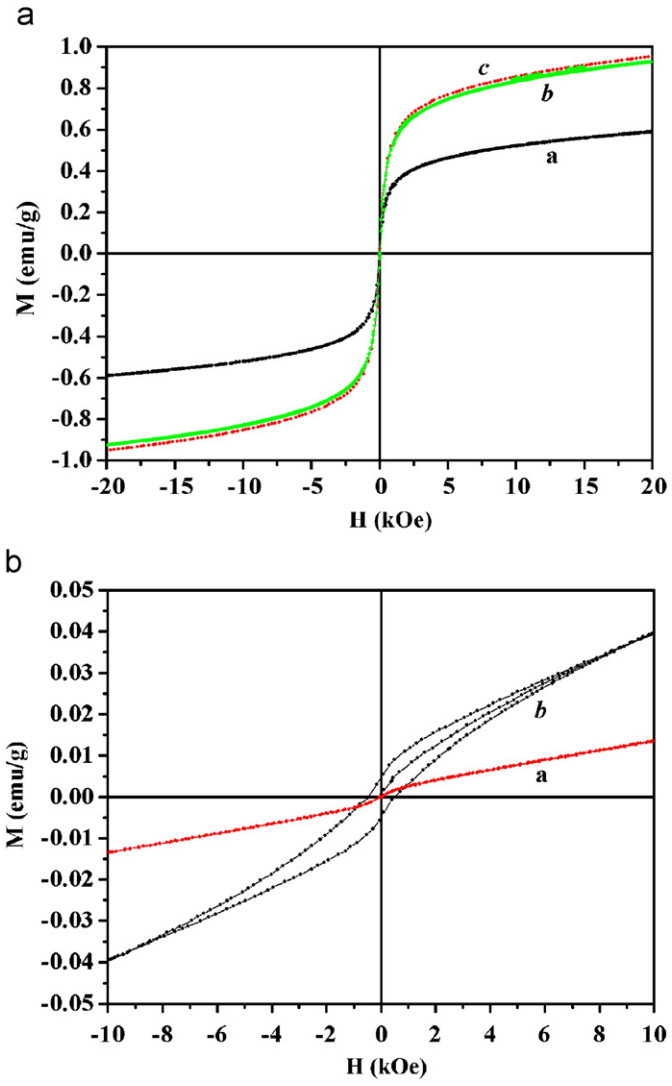

Fig. 4. (a) M–H curves at 305 K for samples $(In_{0.9}Fe_{0.08}Ni_{0.02})_2O_3$ (a), $(In_{0.9}Fe_{0.04}Ni_{0.06})_2O_3$ (b), and $(In_{0.9}Fe_{0.06}Ni_{0.04})_2O_3$ (c); (b) M–H curves at 305 K for samples $(In_{0.9}Ni_{0.1})_2O_3$ (a) and $(In_{0.9}Fe_{0.1})_2O_3$ (b).

bulk samples [12]. The little decrease of saturation magnetization in the sample with $x = 0.06$, compared with the sample with $x = 0.04$, nicely suggests that doping with 6 at% Ni atoms to In_2O_3 host lattice has produced more antiferromagnetic NiO clusters which could offset ferromagnetic moment to some extent. This is consistent with our EXAFS results.

Magnetic-field dependence of magnetization for samples with $x = 0$, 0.1 at room-temperature is illustrated in Fig. 4(b). The sample with $x = 0$ shows open hysteresis loop with coercive force 400 Oe. The saturation magnetization is not reached even at a maximum applied field of 1 T. This observation is consistent with the presence of a paramagnetic particle core (probably due to the Fe atoms doped into cubic In_2O_3 lattice as reported in Ref. [10]), which is superimposed to a net moment due to the intrinsic weak ferromagnetism or Fe_2O_3 clusters [15]. And the intrinsic weak ferromagnetism could be described on the basis of the hexagonal In_2O_3 symmetry and the canting of the two magnetic sublattices, similar to that of bulk hexagonal Fe_2O_3 [15]. Magnetization data of the sample with $x = 0.1$ show no trace of ferromagnetism at room-temperature. It is well known that bulk NiO is antiferromagnetic. Consequently, the paramagnetic behavior in this sample probably originates from the superimposition of the antiferromagnetic and intrinsic ferromagnetic effects.

Our magneto-transport measurements allow us to examine the interactions between charge carriers and magnetic ions. In order to get relative smaller resistivity in the bulk sample, high temperature treatment up to 1000 °C was applied. The magnetic behavior has not been changed as shown in the inset (left) of Fig. 5. Magnetic-field dependence of Hall resistivity ρ_{xy} of the sample is measured, as shown in Fig. 5. The data were obtained by a simple subtraction to eliminate any magnetic-field effects which are even functions of fields, i.e., magnetoresistance (MR) ($\rho_{xy} = 1/2[\rho_{xy}(H^+) - \rho_{xy}(H^-)]$). The data show a sharp increase in ρ_{xy} at low fields, more clearly from the inset (right) of Fig. 5. ρ_{xy} also shows a small linear dependence on μ_oH at high fields. As we all know, Hall resistivity ρ_{xy} in magnetic materials can be expressed as $\rho_{xy} = R_oB + R_sM$, where R_o is the ordinary Hall coefficient, R_s is the anomalous Hall coefficient and M the magnetization of the sample. The small linear slope of the ρ_{xy}–μ_oH curves under high magnetic fields ($\mu_oH = 6$–20 kOe) allowed us to determine R_o. The conduction type was n type and the carrier concentration was about $10^{16}\,cm^{-3}$. Although the concentration is much smaller than that of reported $10^{20}\,cm^{-3}$ [8], it may be high enough to induce dominant ferromagnetic coupling in our samples [16]. Consequently, the observed ferromagnetism in our samples might be explained by the carrier-induced Ruderman–Kittel–Kasuya–Yoshida (RKKY) mechanism [4,16–18].

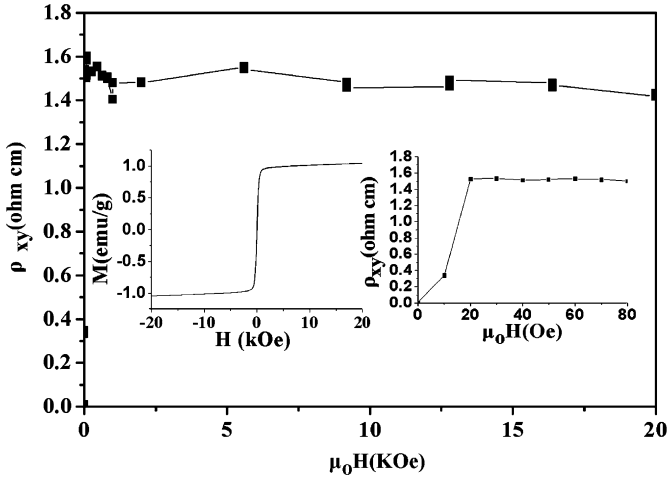

Fig. 5. Hall resistivity versus μ_0H of the bulk sample $(In_{0.9}Fe_{0.06}Ni_{0.04})_2O_3$. Insets: right—magnified view of Hall resistivity at low fields; left—magnetic behavior of the bulk sample $(In_{0.9}Fe_{0.06}Ni_{0.04})_2O_3$ after high-temperature treatment up to 1000 °C for 20 h.

4. Conclusion

In conclusion, polycrystalline Fe- and Ni-co-doped In_2O_3 samples are prepared. All the three co-doped samples $(In_{0.9}Fe_{0.1-x}Ni_x)_2O_3$ ($x = 0.02$, 0.04 and 0.06) were found to be ferromagnetic at room-temperature with enhanced magnetization compared with others. The XRD and EXAFS analyses indicate that the solubility of Fe and Ni atoms in In_2O_3 host lattice is around 10 and 4 at%, respectively. The magneto-transport properties measured on the bulk sample $(In_{0.9}Fe_{0.06}Ni_{0.04})_2O_3$ showed the conduction type is *n* type and the carrier concentration is $10^{16}\,cm^{-3}$.

Acknowledgment

The authors would like to appreciate the financial support from the National Natural Science Foundation of China under Grant No. 50672105, the Hundred Talents Program of the Chinese Academy of Sciences. The support of EXAFS measurements by National Synchrotron radiation at the National Synchrotron Radiation Laboratory in University of Science and Technology of China is gratefully acknowledged.

References

[1] H. Ohno, Making nonmagnetic semiconductors ferromagnetic, Science 281 (1998) 951–956.
[2] Z.J. Wang, W.D. Wang, J.K. Tang, L.D. Tung, L. Spinu, W. Zhou, Extraordinary Hall effect and ferromagnetism in Fe-doped reduced rutile, Appl. Phys. Lett. 83 (2003) 518.
[3] D.P. Norto, S.J. Pearton, A.F. Hebard, N. Thedoropoulou, L.A. Boatner, R.G. Wilson, Ferromagnetism in Mn-implanted ZnO:Sn single crystals, Appl. Phys. Lett. 82 (2003) 239.
[4] K. Ueda, H. Tabata, T. Kawai, Magnetic and electric properties of transition-metal-doped ZnO films, Appl. Phys. Lett. 79 (2001) 988.
[5] F. Tsui, L. He, L. Ma, A. Tkachuk, Y.S. Chu, K. Nakajima, T. Chikyow, Novel germanium-based magnetic semiconductors, Phys. Rev. Lett. 91 (2003) 177203.
[6] J.Y. Kim, J.H. Park, B.G. Park, H.J. Noh, S.J. Oh, J.S. Yang, D.H. Kim, S.D. Bu, T.W. Noh, Ferromagnetism induced by clustered Co in Co-doped anatase TiO_2 thin films, Phys. Rev. Lett. 90 (2003) 017401.
[7] Y.K. Yoo, Q. Xue, H.C. Lee, S. Cheng, X.D. Xiang, G.F. Dionne, S. Xu, J. He, Y.S. Chu, S.D. Preite, S.E. Lofland, I. Takeuchi, Bulk synthesis and high-temperature ferromagnetism of $(In_{1-x}Fe_x)_2O_{3-\sigma}$ with Cu codoping, Appl. Phys. Lett. 86 (2005) 042506.
[8] J. He, S. Xu, Y.K. Yoo, Q. Xue, H.C. Lee, S. Cheng, X.D. Xiang, G.F. Dionne, I. Takeuchi, Room-temperature ferromagnetic *n*-type semiconductor in $(In_{1-x}Fe_x)_2O_{3-\sigma}$, Appl. Phys. Lett. 86 (2005) 052503.
[9] G. Peleckis, X.L. Wang, S.X. Dou, Ferromagnetism in Mn-doped In_2O_3 oxide, J. Magn. Magn. Mater. 301 (2001) 308–311.
[10] G. Pelechis, X.L. Wang, S.X. Dou, Room-temperature ferromagnetism in Mn and Fe codoped In_2O_3, Appl. Phys. Lett. 88 (2006) 132507.
[11] I.-B. Shim, C.S. Kim, S.X. Dou, Doping effect of indium oxide-based diluted magnetic semiconductor thin films, J. Magn. Magn. Mater. 272–276 (2004) e1517–e1572.
[12] G. Peleckis, X.L. Wang, S.X. Dou, High temperature ferromagnetism in Ni-doped In_2O_3 and indium-tin oxide, Appl. Phys. Lett. 89 (2006) 022501.
[13] Ph. Parent, H. Dexpert, G. Tourillon, Structural study of tin-doped indium oxide thin films using X-ray absorption spectroscopy and X-ray diffraction, J. Electrochem. Soc. 139 (1992) 276.
[14] R.W.G. Wycoff, Crystal Structures, vol. 2, Interscience Publishers, New York, 1964, p. 6.
[15] M.F. Hansen, F. Bødker, S. Mørup, Dynamics of magnetic nanoparticles studied by neutron scattering, Phys. Rev. Lett. 79 (1997) 4910.
[16] H.-T. Lin, T.-S. Chin, J.-C. Shilh, S.-H. Lin, T.-M. Hong, Enhancement of ferromagnetic properties in $Zn_{1-x}Co_xO$ by additional Cu doping, Appl. Phys. Lett. 85 (2004) 621.
[17] A. Wolf, D.D. Awschalom, R.A. Buhrman, J.M. Daughton, S.V. Molnar, M.L. Roukes, A.Y. Chtchelkanova, D.M. Treger, Spintronics: a spin-based electronics vision for the future, Science 294 (2001) 1488.
[18] T. Story, R.R. Galazka, Carrier-concentration-induced ferromagnetism in PbSnMnTe, Phys. Rev. Lett. 56 (1986) 777.